Cement & Concrete Composites 30 (2008) 947–956

Contents lists available at ScienceDirect

Cement & Concrete Composites

journal homepage: www.elsevier.com/locate/cemconcomp

Analysis of microcracking induced by differential drying shrinkage

C. de Sa [a], F. Benboudjema [a,*], M. Thiery [b], J. Sicard [a]

[a] Laboratoire de Mécanique et Technologie, Ecole Normale Supérieure de Cachan, 61 Avenue du Président Wilson, 94235 Cachan Cedex, France
[b] Laboratoire Central des Ponts et Chaussées, 58 Boulevard Lefebvre, 75732 Paris, France

ARTICLE INFO

Article history:
Received 30 August 2007
Received in revised form 22 June 2008
Accepted 28 June 2008
Available online 11 July 2008

Keywords:
Drying
Shrinkage
Creep
Cracking
Concrete
Coupling
Modeling

ABSTRACT

The drying of concrete induces surface microcracking. Because drying is, especially, a slow process, differential drying between the surface and the core induces shrinkage, which provokes an increase of the tensile stresses on the surface and of the compressive stresses in the core (the resultant is zero if there are no external forces or external restraints). Often, the tensile stresses obtained by elastic finite element analysis exceed the tensile strength. Numerical simulations show that if creep strains are taken into account the damage due to differential drying shrinkage is less important (compared to the case if creep is not considered in the numerical analysis). Therefore, a little drop of mechanical properties is predicted due to drying, for the studied concrete. Therefore, one may assume that microcracking and the associated drop in the Young's modulus as the concrete dries are due mainly to aggregate restraint. Besides, an elastic damage model for prediction of cracking is found to be sufficient to retrieve evolution of drying shrinkage and damage fields (but not the orientation).

1. Introduction

The drying of concrete parts has structural consequences: differential drying shrinkage induces self-equilibrated stresses, leading to microcracking on the surface. This phenomenon can be observed using an optical or a scanning electron microscope [1–3]. Besides, it is the cement paste alone that shrinks; therefore, the strain is restrained by the aggregates, leading to debonding at the cement paste/aggregate interfaces (circumferential cracks) and to the development of intergranular cracks (radial cracks) [1,4,5].

The orientation of the microcracks on the surface was found to be quasi-isotropic [2,3]. The application of compressive stresses perpendicular to the cracks closes these only partially [3] and destroys the isotropic nature of their orientation. Therefore, this microcracking may lead to orthotropic mechanical behavior of the concrete. The opening of the microcracks is relatively small, between about 0.25 and 50 μm [1,3,6]. Therefore, these cracks can be assumed to have a negligible effect on the material's diffusivity and permeability (only for water transport during drying). This was confirmed by experimental results: similar evolutions of weight loss were measured for loaded and non-loaded drying specimens [7,8].

Drying (and the associated microcracking) seems to have a significant impact on the mechanical properties. Regarding the Young's modulus, most authors report a decrease of between 4% and 30% as concrete dries [9–14]. Conversely, there is no consensus concerning the compressive and tensile strengths: regarding compressive strength, some authors report an increase [10,11,13,14] while others report a decrease [9,15–17]. Concerning tensile strength, a slight increase was found in a splitting test [17] while an initial decrease followed by a progressive increase up to zero percent relative humidity was observed in bending [12,16,18]. A decrease followed by an increase was also measured in direct tensile tests [18,19].

These contradictory results can be explained by different mechanisms which take place as concrete dries:

- superficial tension increases due to the loss of adsorbed water [9]. This mechanism reduces the internal effective compressive stresses in the solid skeleton and, therefore, tends to increase compressive strength;
- capillary pressures increase and act like prestresses. This mechanism, too, tends to increase compressive and tensile strengths;
- microcracking due to differential shrinkage and aggregate restraint contributes to a global loss of mechanical properties. The temperature and size of the specimens being tested as well as the relative ambient humidity affect drying and, consequently, the microcracking of concrete.

Several papers have dealt with the modeling of drying-induced microcracking before (for example, [13,23,26–28]). However, these did not emphasize the effect of creep relaxation or of the type of cracking model.

* Corresponding author. Tel.: +33 1 47 40 53 69; fax: +33 1 47 40 74 65.
E-mail address: farid.benboudjema@dgc.ens-cachan.fr (F. Benboudjema).

0958-9465/$ - see front matter © 2008 Elsevier Ltd. All rights reserved.
doi:10.1016/j.cemconcomp.2008.06.015

The objective of this paper is to study the influence of creep and cracking models on the prediction of microcracking induced by differential drying shrinkage. Drying is modeled through a nonlinear macroscopic diffusion equation [20–22]. Drying-induced shrinkage is assumed to be driven by capillary pressure alone [20]. Basic creep is modeled by means of several parallel Kelvin–Voigt chains. Drying creep model of Bažant and Chern [23] is used. Cracking is described by two models: the first is an isotropic elastic damage model (IED) based on Mazars' model [24]; the other is an orthotropic elastic–plastic damage model (OEPD) previously developed by Benboudjema et al. [25]. Several calculations were performed in order to determine the effects of creep, induced orthotropy and irreversible strain during unloading on the cracking pattern (damage) due to drying and on the residual mechanical properties in compression and in tension.

2. Hydromechanical modeling of concrete

2.1. The drying model

The drying of cement-based materials is a complex phenomenon. Several, more-or-less coupled mechanisms are involved: permeation, diffusion, adsorption–desorption and condensation–evaporation [20].

Drying can be analyzed through the resolution of liquid water, vapor and dry air mass balance equations:

$$\begin{cases} \dot{m}_\mathrm{l} + \mathrm{div}(m_\mathrm{l}\mathbf{v}_\mathrm{l}) = -\dot{m}_\mathrm{vap} \\ \dot{m}_\mathrm{v} + \mathrm{div}(m_\mathrm{v}\mathbf{v}_\mathrm{v}) = \dot{m}_\mathrm{vap} \\ \dot{m}_\mathrm{a} + \mathrm{div}(m_\mathrm{a}\mathbf{v}_\mathrm{a}) = 0 \end{cases} \quad (1)$$

where $m_x = \phi S_x \rho_x$ is the mass of fluid per unit volume (x = l for liquid water, v for vapor and a for dry air); ϕ is the porosity; S_x is the degree of saturation; ρ_x is the density; $\dot{m}_\mathrm{vap}$ is the mass of vaporized water per unit volume and per second; $\mathbf{v}_x$ is the velocity of the fluid.

The velocity of each phase is related to the solid skeleton's strain, diffusion and convection. For "natural" drying (i.e. at ambient temperature), it seems reasonable to assume the following hypothesis [21,22]:

- the effect of the solid skeleton's strain rate on the drying process is negligible; so are the effects of diffusion and convection ($\mathbf{v}_\mathrm{v} = \mathbf{v}_\mathrm{a} = \mathbf{0}$);
- the gas pressure (vapor and dry air) is equal to the atmospheric pressure and is negligible compared to the liquid water and capillary pressures (which equal about −96 MPa at 50% relative humidity). Thus, the capillary pressure and the liquid water pressure are assumed to be equal ($p_\mathrm{c} = p_\mathrm{l}$).

The liquid water velocity can be calculated using Darcy's law:

$$S_\mathrm{l}\phi\mathbf{v}_\mathrm{l} = -\frac{Kk_\mathrm{rl}(S_\mathrm{l})}{\mu_\mathrm{l}} \cdot \vec{\mathrm{grad}}\,(p_\mathrm{l}) = -\frac{Kk_\mathrm{rl}(S_\mathrm{l})}{\mu_\mathrm{l}} \cdot \vec{\mathrm{grad}}\,(p_\mathrm{c}) \quad (2)$$

where K, k_rl and μ_l are, respectively, the intrinsic permeability, the relative permeability and the viscosity of the liquid water. [21,29] showed that this equation is sufficient for an accurate prediction of the drying of ordinary and high-performance concretes at 20 °C with a relative humidity greater than 50%. For more porous concretes, the contribution of the vapor phase transport can no longer be neglected [29].

Using Eqs. (1) and (2) and the previous hypothesis, one obtains the following equation for the evolution of the capillary pressure:

$$\frac{\mathrm{d}S_\mathrm{l}}{\mathrm{d}p_\mathrm{c}}\frac{\mathrm{d}p_\mathrm{c}}{\mathrm{d}t} = \mathrm{div}\left(k_\mathrm{rl}(S_\mathrm{l})\frac{K}{\mu_\mathrm{l}\phi}\cdot\mathrm{grad}(p_\mathrm{c})\right) \quad (3)$$

The degree of saturation is related to the capillary pressure through van Genuchten's relation [30]:

$$p_\mathrm{c}(S_\mathrm{l}) = a\left(S_\mathrm{l}^{-b} - 1\right)^{1-1/b} \quad (4)$$

where a and b are parameters of the material. One should note that this model was initially developed for soils, but has been used successfully for concrete several times (for example, [20–22]).

The relative permeability is also related to the degree of saturation through van Genuchten's relation [30]:

$$k_\mathrm{rl}(S_\mathrm{l}) = \sqrt{S_\mathrm{l}}\left[1 - \left(1 - S_\mathrm{l}^{b}\right)^{1/b}\right] \quad (5)$$

Drying can also be modeled in the same way using a nonlinear diffusion-type equation expressed in terms of relative humidity or water content (for example, [31,32]).

2.2. The drying shrinkage model

The drying shrinkage model is based on the capillary pressure mechanism, which seems to prevail in the 50–100% relative humidity range [33].

The capillary pressure can be calculated using Kelvin's law, which assumes equilibrium between the liquid and the water vapor:

$$p_\mathrm{c} = p_\mathrm{l} - p_\mathrm{g} = \frac{\rho_\mathrm{l} RT}{M_\mathrm{w}}\ln(h) \quad (6)$$

where R is the perfect gas constant, T the absolute temperature, h the relative humidity and M_w the molar mass of water.

The capillary pressure is assumed to act upon the solid skeleton on a macroscopic scale by means of a pore pressure p_sol (the effect of the gas pressure is neglected, see Fig. 1):

$$p_\mathrm{sol} = \alpha_\mathrm{ds} S_\mathrm{l} p_\mathrm{c} \quad (7)$$

where α_ds can be viewed as a homogenized coefficient which can be identified from the evolution of the drying shrinkage.

Then, the drying shrinkage strain, which results from the pore pressure, can be calculated using the following equation [20]:

$$\mathrm{d}\varepsilon_\mathrm{ds} = \frac{1-2\nu}{E}\alpha_\mathrm{ds} S_\mathrm{l}\mathrm{d}p_\mathrm{c} \quad (8)$$

This model can be expanded by taking into account the creep strain due to the capillary pressure [34] or the disjoining pressure [35]. Drying shrinkage can also be modeled phenomenologically, i.e. as a proportion of the water content or of the variation of relative humidity (for example, [23,26,36,37]).

2.3. The basic creep model

Many mechanisms have been proposed in order to reproduce all the collected experimental data concerning the basic creep of con-

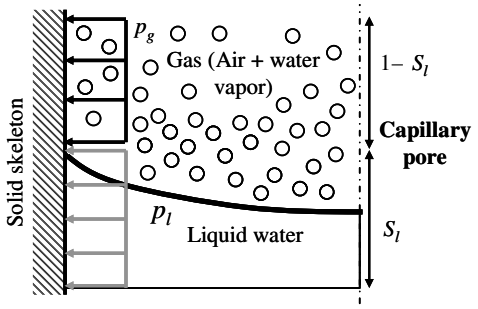

Fig. 1. Capillary pressure.

crete, but no single mechanism has been universally accepted yet. Several models can be found in the literature.

Several basic creep models are based on rheological elements (springs and dashpots). The most popular elements consist of Kelvin–Voigt and Maxwell chains which are combined in series and/or in parallel. In this paper, we use several Kelvin–Voigt chains (Fig. 2). The use of such elements leads to straightforward formulas for the calculation of the evolution of strain, in contrast to Maxwell chains, for example, which require the use of an algorithm such as the exponential algorithm proposed by Bažant and Wu [38]. However, such a model is incapable of predicting irreversible basic creep strains at unloading, which account for about 60–70% of the total creep strain.

Let us consider a Kelvin–Voigt unit i. The evolution of the basic strain is given by the relation:

$$\eta^i_{\mathrm{bc}}\dot{\varepsilon}^i_{\mathrm{bc}}(t) + k^i_{\mathrm{bc}}\varepsilon^i_{\mathrm{bc}}(t) = \tilde{\sigma}(t) \tag{9}$$

where $\tilde{\sigma}(t)$ is the effective stress (see Section 2.5), $\varepsilon^i_{\mathrm{bc}}(t)$ the elementary basic creep strain, k^i_{bc} the stiffness and η^i_{bc} the viscosity of Kelvin–Voigt unit i. The characteristic time is defined as $\tau^i_{\mathrm{bc}} = \frac{\eta^i_{\mathrm{bc}}}{k^i_{\mathrm{bc}}}$. Then, the total basic creep strain is obtained as the sum of all the elementary basic creep strains:

$$\varepsilon_{\mathrm{bc}}(t) = \sum_i \varepsilon^i_{\mathrm{bc}}(t) \tag{10}$$

A short-coming of this approach is that aging was not considered in our study, although it has a considerable influence on basic creep of concrete (for example, [38]). Therefore, this basic creep model is intended to be used only for a specific age at loading. If a different age is to be considered, the model's parameters should be identified again.

2.4. The drying creep model

Drying creep corresponds to the additional strain observed when concrete is under stress and a change in the internal moisture state occurs. This behavior, called the Pickett effect [39], is quite paradoxical. Indeed, a previously dried specimen creeps less than a saturated specimen, even though during a creep test concrete creep rises as the relative humidity decreases [40].

Two mechanisms explain drying creep in concrete. The first mechanism is the microcracking effect [27], which we do take into account since we are using a cracking model (see Section 2.5). The second mechanism is intrinsic. We will be using the stress-induced shrinkage model proposed by Bažant and Chern [23]:

$$\dot{\boldsymbol{\varepsilon}}_{\mathrm{dc}} = \mu|\dot{h}|\tilde{\boldsymbol{\sigma}} \tag{11}$$

where $\boldsymbol{\varepsilon}_{\mathrm{dc}}$ is the stress-induced shrinkage strain and μ a material parameter.

2.5. The cracking model

Two smeared cracking models will be used and compared. The first is an isotropic elastic damage model (IED) based on that proposed by Mazars [24]and described in Reviron et al. [41]. The other is an orthotropic elastic–plastic damage model (OEPD) which we developed in a previous paper [25]. The objective is to study the effects of taking into account (or not) irreversible strains during unloading along with isotropy/orthotropy on the cracking pattern due to drying and on the residual mechanical properties after drying. Since the constitutive relations of these models and the associated algorithms have already been published, we will review them only briefly.

In both models, a characteristic length is introduced in order to avoid mesh dependency [42]. This characteristic length is related to the mesh size [43,44], so that the same amount of energy is dissipated after mesh refinement, when strains are localized in a single row of finite elements.

Numerical implementation of IED model is straightforward. Indeed, all involved equations are defined analytically and can be calculated without any local iteration, which enhances the speed of calculations. This is not the case with OEPD model, which needs local iteration.

2.5.1. The IED model

A scalar damage variable D is used to describe the occurrence of microcracking and the associated degradation of the Young's modulus. The apparent stresses $\boldsymbol{\sigma}$ read:

$$\boldsymbol{\sigma} = (1-D)\cdot\tilde{\boldsymbol{\sigma}} = \mathbf{E}_0\cdot(1-D)\cdot\boldsymbol{\varepsilon}_{\mathrm{e}} \tag{12}$$

where $\boldsymbol{\varepsilon}_{\mathrm{e}}$ are the elastic strains, $\boldsymbol{\varepsilon}$ the total strains and $\mathbf{E}_0$ the elastic stiffness tensor. The elastic strain is

$$\dot{\boldsymbol{\varepsilon}}_{\mathrm{e}} = \dot{\boldsymbol{\varepsilon}} - \dot{\boldsymbol{\varepsilon}}_{\mathrm{ds}} - \dot{\boldsymbol{\varepsilon}}_{\mathrm{bc}} - \dot{\boldsymbol{\varepsilon}}_{\mathrm{dc}} \tag{13}$$

The damage criterion f is given by (Fig. 3)

$$f = \hat{\varepsilon} - \kappa_0 \tag{14}$$

where κ_0 is the tensile strain threshold and $\hat{\varepsilon}$ the equivalent tensile strain [24]:

$$\hat{\varepsilon} = \sqrt{\langle\boldsymbol{\varepsilon}_{\mathrm{e}}\rangle_+ : \langle\boldsymbol{\varepsilon}_{\mathrm{e}}\rangle_+} \tag{15}$$

The damage variable is related to the compressive and tensile damage variable by the relation:

$$D = (1-\alpha_{\mathrm{t}})D_{\mathrm{c}} + \alpha_{\mathrm{t}}D_{\mathrm{t}} \tag{16}$$

where α_{t} is related to the tensile and compressive strains created by the principal tensile and compressive stresses [24].

The evolution of the damage variables in tension D_{t} and in compression D_{c} reads:

$$D_x = 1 - \frac{\kappa_0}{\hat{\varepsilon}}\left[(1+A_x)\exp(-B_x\hat{\varepsilon}) - A_x\exp(-2B_x\hat{\varepsilon})\right] \tag{17}$$

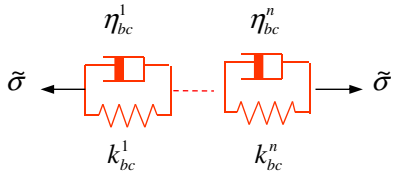

Fig. 2. Basic creep model.

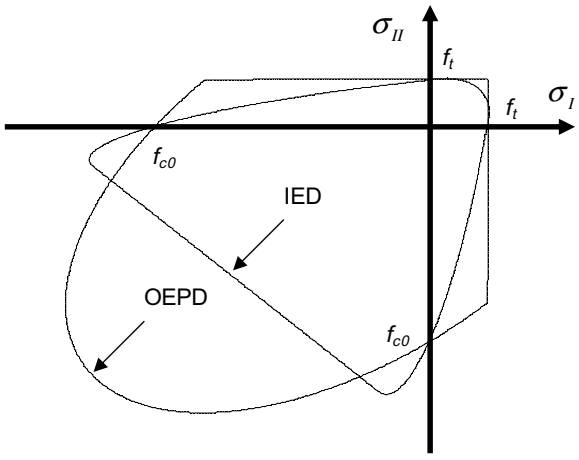

Fig. 3. Yield surfaces in plane stresses conditions for both IED and OEPD models.

where x = t for tension and x = c for compression, and A_x and B_x are constant material parameters which control the nonlinear part of the stress–strain curve.

2.5.2. The OEPD model

As in the IED model, damage theory is used to describe the degradation of the Young's modulus. Now, the damage process is assumed to be isotropic in compression and orthotropic in tension, where orthotropy is induced by cracking in preferential directions which occurs during drying. The damage tensor $\mathbf{D}$ is divided into a compressive scalar part D_c and a tensile tensor part $\mathbf{D}_t$:

$$\mathbf{1} - \mathbf{D} = (1 - D_c)(\mathbf{1} - \mathbf{D}_t) \tag{18}$$

The evolution of damage is considered to be related to the relative crack opening resulting from the accumulated plastic strains κ_c and $\hat{\kappa}_t^i$ (used as hardening/softening parameters, $i \in [1,3]$) given by

$$D_c = 1 - \exp(-c_c\kappa_c) \text{ and } D_t^{ii} = 1 - \exp(-c_t\hat{\kappa}_t^i) \tag{19}$$

where c_t and c_c are material parameters identified from experimental stress–strain curves.

Here, the use of plasticity theory enables the description of inelastic strains $\boldsymbol{\varepsilon}_p$. In order to obtain a suitable behavior, a Drucker-Prager criterion in compression and three Rankine criteria in tension [45] are used (Fig. 3):

$$\begin{aligned} &F_c(\tilde{\boldsymbol{\sigma}}, \kappa_c) = \sqrt{3J_2(\tilde{\boldsymbol{\sigma}})} + \alpha_f I_1(\tilde{\boldsymbol{\sigma}}) - \beta\tilde{\tau}_c(\kappa_c) \text{ and} \\ &F_t^i(\hat{\tilde{\boldsymbol{\sigma}}}, \hat{\kappa}_t^i) = \hat{\tilde{\boldsymbol{\sigma}}}^i - \tilde{\tau}_t^i(\hat{\kappa}_t^i) \end{aligned} \tag{20}$$

where I_1 and J_2 are the first and second invariants, $\tilde{\tau}_c$ the effective strength in compression related to the compressive accumulated plastic strain κ_c, α_f and β two material parameters which depend on the ratio of the uniaxial to the biaxial compressive strengths, and $\tilde{\tau}_t^i$ the corresponding effective strength related to the accumulated tensile plastic strain vector $\hat{\kappa}_t^i$.

The effective strength of the material in tension as well as in compression is

$$\tilde{\tau}_c(\kappa_c) = \tau_c(\kappa_c)/(1 - D_c) \text{ and } \tilde{\tau}_t^i(\hat{\kappa}_t^i) = \tau_t^i(\hat{\kappa}_t^i)/(1 - D_t^{ii}) \tag{21}$$

where τ_c and τ_t^i are the nominal strengths of the material, defined by exponential functions:

$$\begin{aligned} \tau_c &= f_{c0}[(1 + a_c)\exp(-b_c\kappa_c) - a_c\exp(-2b_c\kappa_c)] \\ \tau_t^i &= f_t\left[(1 + a_t)\exp\left(-b_t\hat{\kappa}_t^i\right) - a_t\exp\left(-2b_t\hat{\kappa}_t^i\right)\right] \end{aligned} \tag{22}$$

a_c and b_c are material parameters identified from a uniaxial compression test; f_{c0} is the elastic strength in compression; a_t and b_t are material parameters identified from a uniaxial tension test; f_t is the elastic strength in tension.

Then, the stress–strain relation becomes:

$$\boldsymbol{\sigma} = (\mathbf{I} - \mathbf{D}) \cdot \tilde{\boldsymbol{\sigma}} = (\mathbf{I} - \mathbf{D}) \cdot \mathbf{E}_0 \cdot \boldsymbol{\varepsilon}_e \tag{23}$$

The elastic strain is:

$$\dot{\boldsymbol{\varepsilon}}_e = \dot{\boldsymbol{\varepsilon}} - \dot{\boldsymbol{\varepsilon}}_p - \dot{\boldsymbol{\varepsilon}}_{ds} - \dot{\boldsymbol{\varepsilon}}_{bc} - \dot{\boldsymbol{\varepsilon}}_{dc} \tag{24}$$

Where the plastic strain $\boldsymbol{\varepsilon}_p$ is obtained by Koiter assumption:

$$\dot{\boldsymbol{\varepsilon}}^p = \sum_i \dot{\lambda}_t^i \frac{\partial F_t^i}{\partial \tilde{\boldsymbol{\sigma}}} + \dot{\lambda}_c \frac{\partial G_c}{\partial \tilde{\boldsymbol{\sigma}}} \tag{25}$$

where λ_t^i and λ_c are the tensile and compressive plastic multipliers, respectively, which gives the cumulated plastic strain rates as

$$\dot{\kappa}_c = \left(1 + 2\alpha_g^2\right)^{1/2}\dot{\lambda}_c \text{ and } \dot{\hat{\kappa}}_t^i = \dot{\lambda}_t^i \tag{26}$$

A non-associative plastic potential is adopted in compression in order to predict the correct amount of dilatancy of concrete since damage is isotropic in compression:

$$G_c = \sqrt{3J_2(\tilde{\boldsymbol{\sigma}})} + \alpha_g I_1(\tilde{\sigma}) - \beta\tilde{\tau}_c(\kappa_c) \tag{27}$$

where α_g is a material parameter which controls the dilatancy of concrete.

3. Numerical simulations

The main objective is to study the effect of creep and some mechanical properties (isotropy/orthotropy, inelastic strain) on the predicted cracking pattern and mechanical parameters (Young's modulus, compressive and tensile strength) after drying. Unfortunately, no single experiment (i.e., corresponding to one concrete mix) is available in the literature to carry out this study in the most appropriate way. Nevertheless, a significant amount of information is available through the tests performed by Granger [46] and will be used here. A brief description of these tests is first presented.

The experiments were carried out on 28-day-old specimens (normal concrete with a water-to-cement ratio of 0.56), which had been previously sealed. The drying tests were performed in a room at constant temperature (20 °C ± 1 °C) and constant relative humidity (50% ± 5%). The weight loss was measured on 16 cm × 15 cm (diameter × height) cylindrical specimens. Shrinkage and creep tests were performed on 16 cm × 100 cm (diameter × height) cylindrical specimens. The displacements were measured on a 50-cm middle section of the specimens in order to avoid boundary effects. For the basic and total creep tests, a compressive stress of 12 MPa was applied. The mechanical properties measured at 28 days were the Young's modulus E = 33.7 GPa, the Poisson's ratio ν = 0.248, the compressive strength f_c = 41 MPa, and the tensile strength f_t = 3.5 MPa.

The simulations were carried out using the finite element code CAST3M developed by the French Atomic Energy Commission [47]. An axisymmetric model composed of eight-node rectangular finite elements was used. The mesh and boundary conditions are presented in Fig. 4. One can observe that the mesh is more refined along the drying side of the sample.

First, we will present the identification of the material parameters. Then, we will discuss the predictive numerical simulations which were performed in order to reach our objective.

3.1. Identification of the material parameters

3.1.1. Evolution of drying

First, since no such information was available for the concrete being studied, isothermal desorption parameters (van Genuchten's model, see Eq. (4)) were identified from a similar concrete mix (Philajavaara [16], Fig. 5).

Then, the intrinsic permeability was identified from the experimental evolution of the weight loss (Granger [46], Fig. 6). The material parameters are given in Table 1.

3.1.2. Static mechanical behavior

Typical stress–strain curves in compression and tension (Figs. 7 and 8; Table 2) were used for both models (IED and OEPD, see Sections 2.5.1 and 2.5.2). The only difference between the two curves concerns the unloading phase.

3.1.3. Basic and drying creep

Basic creep parameters were identified separately using basic creep experimental results. Five Kelvin–Voigt elements were needed to fit the whole range of experimental results with good accuracy. Then, the drying creep parameter was identified from the experimental evolution of the basic and drying creep strains.

Figs. 9 and 10 show the simulated (longitudinal) basic and drying creep strain obtained by fitting the experimental curve with the set of parameters given in Table 3.

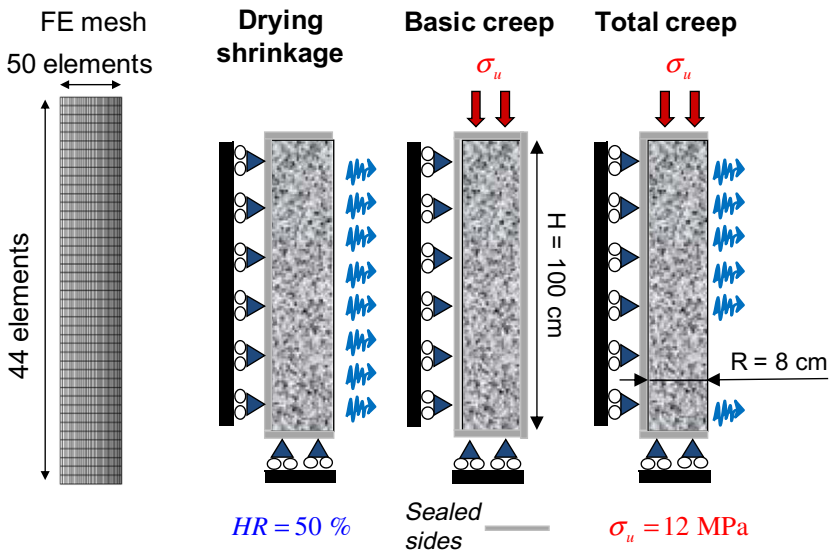

Fig. 4. Finite element discretization and boundary conditions for the simulation of drying shrinkage, basic creep and total creep tests (axisymmetric configuration).

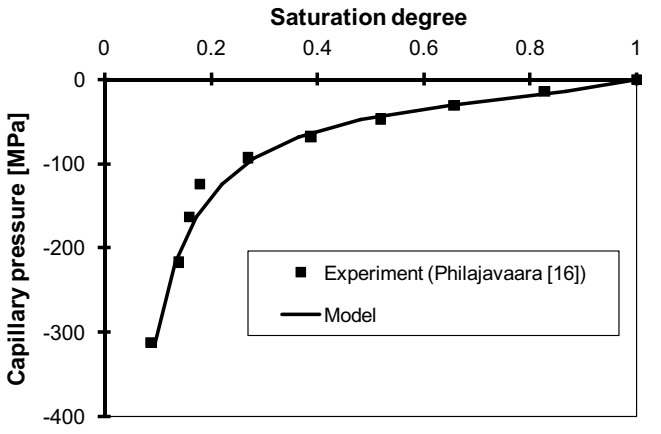

Fig. 5. Identification of drying model parameters – experimental (Philajavaara [16]) and numerically fitted evolutions of capillary pressure with respect to the degree of saturation.

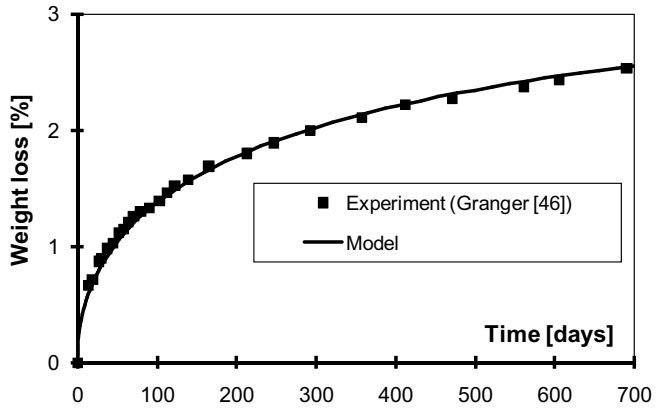

Fig. 6. Identification of drying model parameters – experimental (Granger [46]) and numerically fitted evolutions of the weight loss with time.

Table 1
Parameters of the drying model used in the numerical simulation

a (MPa)	B	ϕ	K (m^2)
25	2.08	0.13	1.1×10^{-21}

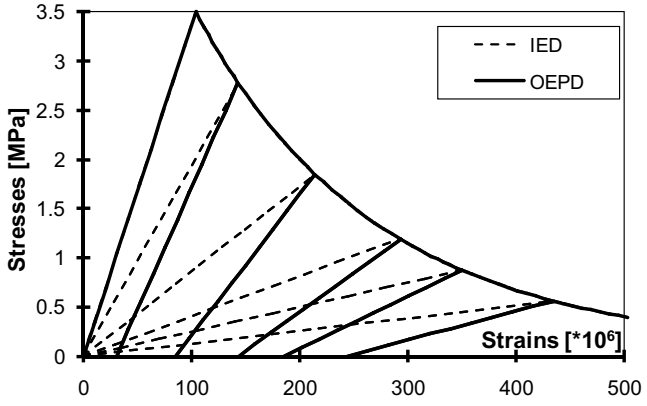

Fig. 7. Stress–strain curves in tension for the two models.

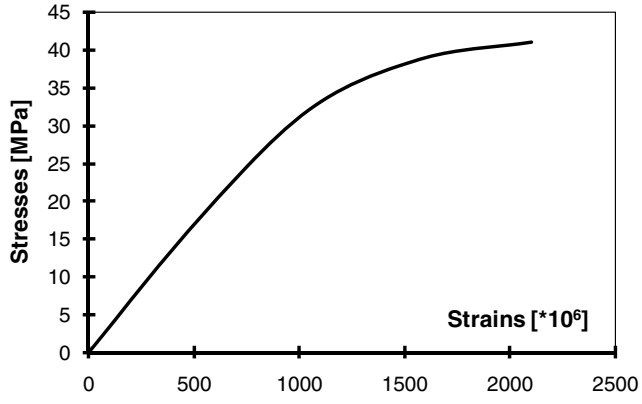

Fig. 8. Stress–strain curve in compression for the two models.

Table 2
Mechanical parameters for the two models

A_t	B_t	A_c	B_c	κ_0	f_{c0} (MPa)	α_f
−0.2	5×10^3	14.4	920	1.04×10^{-4}	16.4	0.14
a_t	b_t	c_t	a_c	b_c	c_c	β
8.25×10^{-3}	7.5×10^3	10^4	7.87	430	240	0.86

3.1.4. Drying shrinkage

Finally, α_{ds} (Eq. (7), Table 3) was identified from the experimental evolution of drying shrinkage. The evolution of the drying shrinkage strain with respect to the weight loss is shown in Fig. 11 for three different models. The type of mechanical model has only a small influence on the evolution of drying shrinkage. The effect of creep is more pronounced. Indeed, due to the relaxation of the stresses, the predicted damage is less when creep is taken into account (see also Section 3.2.1). Therefore, the elastic and inelastic tensile strains caused by the opening of the cracks are smaller, which results in greater apparent drying shrinkage (compressive strain).

3.2. Numerical analysis of the influence of the mechanical model and of creep

The material parameters identified previously were used in order to study the influence of the mechanical model and of creep on the predicted microcracks (magnitude and orientation) and mechanical properties after 700 days of drying.

3.2.1. Damage after drying

The damage field after 700 days of drying is shown in Fig. 12 for three different models. The effect of creep is significant. Indeed, creep tends to relax the predicted stresses, which results in a smaller damaged thickness (about 1.8 cm when creep is not taken into account compared to about 7 mm when creep is taken into account). This is relatively small compared to the experimental observation by Bisschop and van Mier [1] (about 2 cm for a 4-cm-wide specimen at 30% RH). However, the models did not take into account aggregate restraint, which seems to play an important role in the development of cracks during drying (see the next section).

The effect of the mechanical model is less significant. The difference observed results from the different static behavior after unloading in tension (Fig. 7). For a given tensile strain, the damage (related to the slope) is less when the inelastic strain is taken into account.

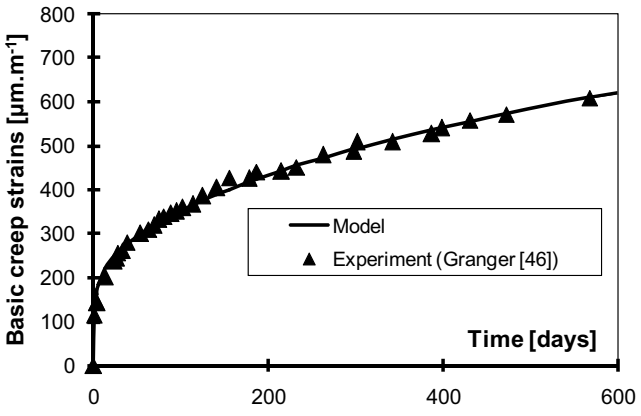

Fig. 9. Experimental and numerically fitted evolutions of the longitudinal basic creep strain with time.

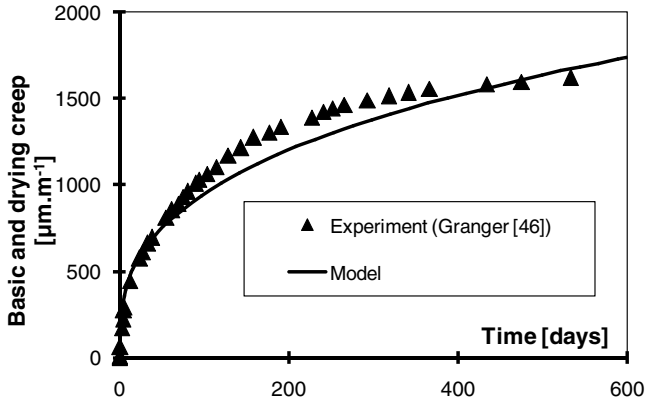

Fig. 10. Experimental and numerically fitted evolutions of the total longitudinal delayed strain with time.

Table 3
Material parameters for the drying shrinkage, basic creep and drying creep models

k^1_{bc} (GPa)	τ^1_{bc} (days)	k^2_{bc} (GPa)	τ^2_{bc} (days)	k^3_{bc} (GPa)	τ^3_{bc} (days)
169.4	0.1	168	1	157.3	10
k^4_{bc} (GPa)	τ^4_{bc} (days)	k^5_{bc} (GPa)	τ^5_{bc} (days)	μ (GPa^{-1})	α_{ds}
105.2	100	18.6	1000	0.3	1.2

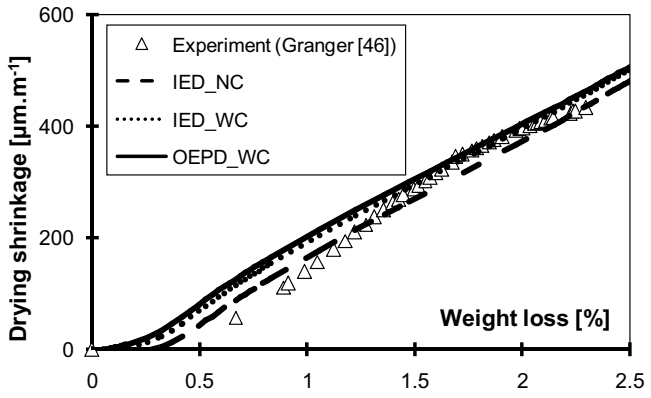

Fig. 11. Experimental and simulated drying shrinkage as functions of the weight loss for the two mechanical models (NC = without taking creep into account; WC = taking basic and drying creep into account).

A difference in the orientation of the microcracks was also observed. Indeed, the radial damage D_{rr} was equal to zero while the vertical and orthoradial damage parameters D_{zz} and $D_{\theta\theta}$, were almost identical. This means that microcracking on the surface of the cylinder is nearly isotropic (in 2D). This agrees with the experimental results of Sicard et al. [3], shown in Fig. 13 with the associated orientation of the predicted damage values (OEPD taking creep into account).

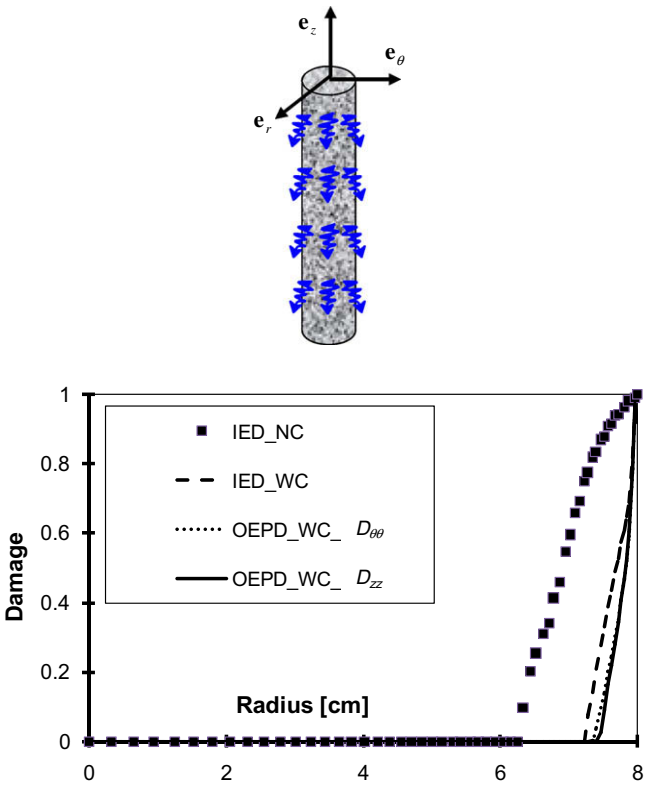

Fig. 12. Damage as a function of the radius after 700 days of drying for the two mechanical models (NC = without taking creep into account; WC = taking basic and drying creep into account).

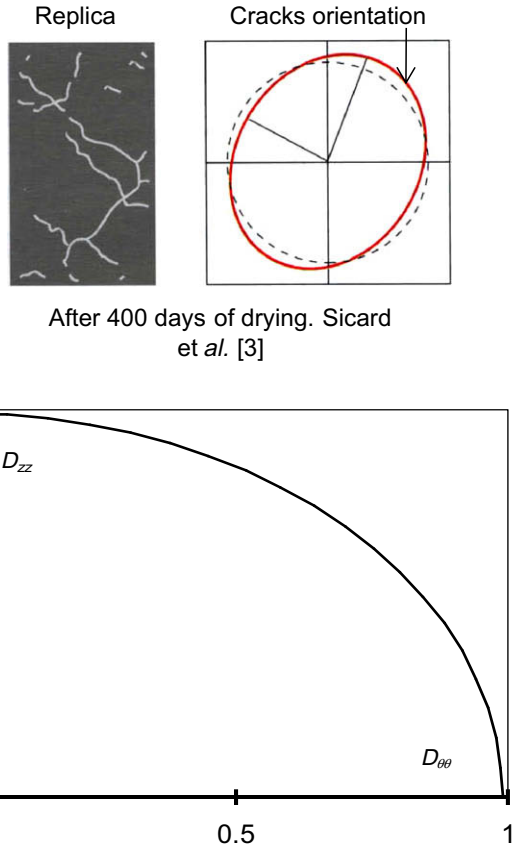

Fig. 13. Orientation of the cracks (left) and damage (right) at the surface of the specimen after 700 days of drying (OEPD + WC).

3.2.2. Effect of drying-induced cracking on the mechanical properties

As seen previously, drying induces microcracking on the surface of concrete. Therefore, a loss of mechanical properties can be expected after drying. Tensile or compressive loading was applied on the top side of the specimens after 700 days of drying. Fig. 12 also shows that the predicted damage depends significantly on the model being used. The effect of drying on the mechanical properties is given in Table 4 for three different models. This leads to the following remarks:

1. when creep is not taken into account, the predictions show a significant drop in Young's modulus, compressive strength and tensile strength (between 35% and 73%). This does not agree with the experimental results;
2. when creep alone is taken into account (but not inelastic strain or induced orthotropy), a slight decrease (between 4% and 16%) is predicted;
3. when creep strains, inelastic strains and induced orthotropy are all taken into account, the predicted decrease is even less (between 1% and 6%).

From these numerical results, creep seems to have an important effect on the prediction of cracking pattern and associated loss of mechanical properties. Therefore, creep should be taken into account in such analysis.

The last model (OEPD + creep) can be considered to be the most representative of the behavior of concrete. Unfortunately, the results obtained do not agree completely with the experimental data. In the introduction, we mentioned that most authors measured a greater drop in Young's modulus (between 4% and 30%) than we obtained (between 2% and 5%). Concerning the compressive and tensile strengths, there is no consensus. Our numerical simulations predict a drop of 1% and 6%, respectively. For a better prediction of microcracking and the mechanical properties, one should also take into account aggregate restraint (through an additional damage mechanism, as in [28]) and the influence of capillary pressure (through an increase in strength, as in [13]).

Table 4
Effect of drying on the mechanical properties (at 50% RH)

	E/E_0[a] in compression	E/E_0[a] in tension	f_c/f_{c0}[a]	f_t/f_{t0}[a]
IED[b] + NC[c]	0.65	0.54	0.73	0.37
IED[b] + WC[c]	0.92	0.92	0.96	0.84
OEPD[b] + WC[c]	0.98	0.95	0.99	0.94

Influence of the model type.

[a] The subscript 0 denotes initial value (sealed specimens). E, f_c and f_t are the Young's modulus, the compressive strength and the tensile strength, respectively, after drying at 50% HR.

[b] IED = isotropic elastic damage model (see Section 2.5.1); OEPD = orthotropic elastic–plastic damage model (see Section 2.5.2).

[c] NC = without taking creep into account; WC = taking basic creep and drying creep into account.

3.2.3. Analysis of induced orthotropy

Sicard et al. ([3], Fig. 14) observed that an application of vertical compressive stresses induces a modification of the orientation of the microcracks. A significant decrease in horizontal microcracks was measured. The orientation of the predicted damage values (OEPD with creep) after drying under compressive loading is shown in Fig. 14. Such a phenomenon could not be predicted using an isotropic damage model.

The use of an isotropic damage model would yield another misleading result. Let us consider the case of a square specimen (40×40 mm^2, Fig. 15) which is allowed to dry for 700 days on only

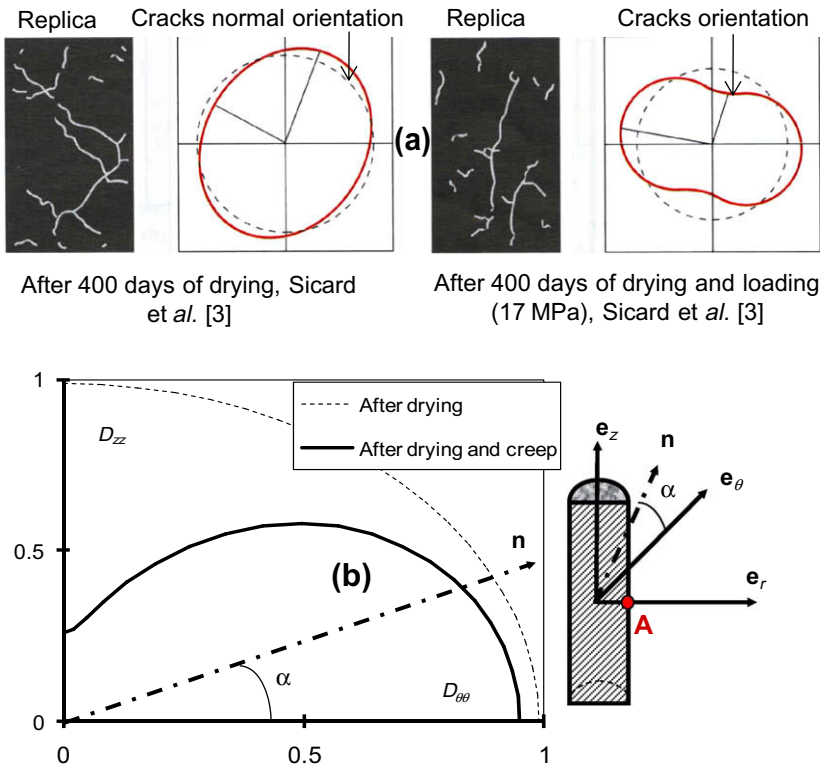

Fig. 14. Orientations of the cracks (a) and projection of damage tensor on a vector **n** (b) at the surface (dot A) of the specimen after 700 days of drying under compression loading (OEPD + WC).

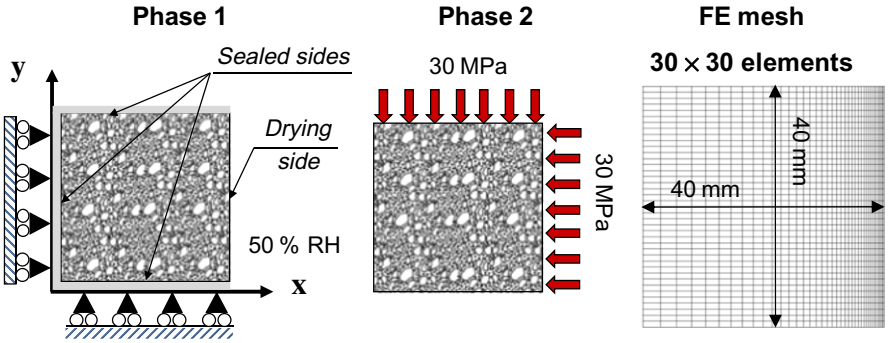

Fig. 15. Boundary conditions, dimensions and finite element mesh.

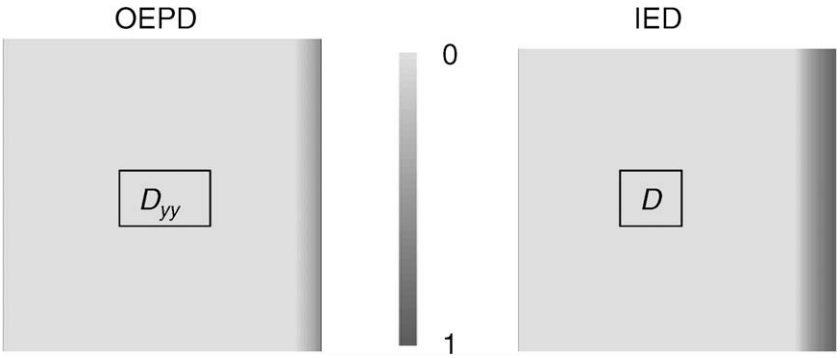

Fig. 16. Damage fields after 700 days of drying for the IED and OEPD models including creep.

one side (Phase 1), and is then loaded in biaxial compression (Phase 2). The numerical simulations were carried out under plane stress conditions, based on experiments performed by Bourgeois et al. [48].

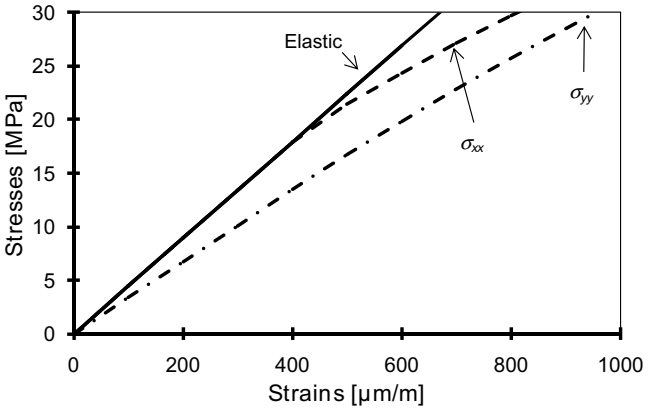

Fig. 17. Stress–strain curves for the OEPD model after 700 days of drying.

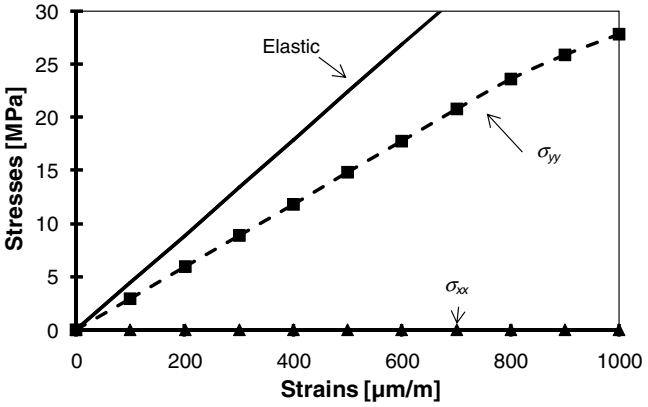

Fig. 18. Stress–strain curves for the IED model after 700 days of drying.

The damage fields after 700 days of drying obtained with both the OEPD and IED models (with creep) are shown in Fig. 16. These fields are similar in terms of amplitude and width, but with the OEPD model the damage variable D_{xx} is equal to zero. This considerably affects the numerical prediction of the residual mechanical properties (see below).

The stress–strain curves obtained with the two models are shown in Figs. 17 and 18. As measured experimentally, different stress–strain curves in the x and y directions after drying are predicted by both models. Thus, drying in a preferential direction makes the behavior of concrete orthotropic. The results obtained with the IED model are not physically correct because they express that the material is unable to sustain a horizontal loading. This is due to the presence of a vertical (isotropic) damage band within which the material is completely damaged (D is equal to 1). With the OEPD model, the horizontal loading is not influenced by the damage variable D_{yy}: one reverts back to the initial stress–strain law. However, the vertical mechanical properties are slightly affected, as discussed previously in Section 3.1.2. These numerical results (obtained by OEPD model with creep) are qualitatively similar to those obtained experimentally by Bourgeois et al. [48].

4. Conclusions

Our numerical simulations highlight the importance of basic and drying creep in the prediction of microcracking induced by differential drying shrinkage. Damage is restricted to only a thin surface layer of the concrete specimen (for the studied concrete mix). Creep also influences the evolution of the residual mechanical properties to a great extent. We found that when creep is taken into account in numerical simulations, damage due to a gradient of drying shrinkage has only a negligible influence on the mechanical properties in the conditions which have been considered in this paper (no external restrain). If creep is not taken into account, the predicted loss of mechanical properties is greater than that measured experimentally. Therefore, a simulation which would not take creep into account could lead to wrong results (i.e. misleading cracking pattern and associated loss of residual mechanical properties).

In some cases, the use of an isotropic damage model for the description of microcracking can also lead to misleading results. The numerical simulations performed enable one to choose which mechanical model (isotropic or orthotropic, with or without inelastic strains) is the most appropriate for the required objectives.

Drying shrinkage strain (but not their consequences) can be predicted accurately using an isotropic elastic damage model without taking creep into account.

An even more accurate prediction of microcracking and of the residual mechanical properties after drying should take into account the effects of aggregate restraint, concrete mix (and especially paste volume [49]) and capillary pressure. Indeed, additional damage occurs due to the shrinkage of cement paste restrained by aggregates, while capillary pressure contributes to the increase in compressive and tensile strength of the material. Corresponding developments are currently underway.

References

[1] Bisschop J, van Mier JGM. How to study drying shrinkage microcracking in cement-based materials using optical and scanning electron microscopy. Cement Concrete Res 2002;32:279–87.
[2] Colina H, Acker P. Drying cracks: kinematics and scale laws. Mater Struct 2000;33:101–7.
[3] Sicard V, François R, Ringot E, Pons G. Influence of creep and shrinkage on cracking in high strength concrete. Cement Concrete Res 1992;22:159–68.
[4] Hearn N. Effect of shrinkage and load-induced cracking on water permeability of concrete. ACI Mater J 1999;96(2):234–41.
[5] Goltermann P. Mechanical predictions of concrete deterioration – Part 2: classification of crack patterns. ACI Mater J 1995;92(1):58–63.
[6] Bažant ZP, Sener S, Kim JK. Effect of cracking on drying permeability and diffusivity of concrete. ACI Mater J 1986;84:351–7.
[7] Hansen TC. Creep of concrete: the influence of variations in the humidity of ambient atmosphere. In: Proceedings 6th congress of the international association of bridge and structural engineering, Stockholm; 1960. p. 57–65.
[8] Lassabatère T, Torrenti J-M, Granger L. Sur le couplage entre séchage du béton et contrainte appliqué. In: Proceedings actes du symposium Saint-Venant, Paris; 1997. p. 331–8 [in French].
[9] Wittmann FH. Einfluβ des feuchtigkeitsgehaltes auf das kriechen des zementsteines. Rheol Acta 1970;9(2):282–7. [in Deutsch].
[10] Brooks JJ, Neville AM. A comparison of creep, elasticity and strength of concrete in tension and in compression. Mag Concrete Res 1977;29(100):131–41.
[11] Dantec P, Terme G. Séchage et comportement différé du béton: influence de la cinétique de dessiccation sur le comportement mécanique des bétons. 1.41.02.5 LCPC Report; 1996 [in French].
[12] Kanna V, Olson RA, Jennings HM. Effect of shrinkage and moisture content on the physical characteristics of blended cement mortars. Cement Concrete Res 1998;18(10):1467–77.
[13] Burlion N, Bourgeois F, Shao J-F. Effects of desiccation on mechanical behaviour of concrete. Cement Concrete Compos 2007;27:367–79.
[14] Yurtdas I, Peng H, Burlion N, Skoczylas F. Influences of water by cement ratio on mechanical properties of mortars submitted to drying. Cement Concrete Res 2006;36:1286–93.
[15] Torrenti J-M. Comportement multiaxial du béton: aspects expérimentaux et modélisation. PhD thesis, Marne-La-Vallée, Ecole Nationale des Ponts et Chaussées; 1987 [in French].
[16] Philajavaara SE. A review of some of the main results of a research on the aging phenomena of concrete: effect of moisture conditions on strength, Shrinkage and creep of mature concrete. Cement Concrete Res 1974;4(5):761–71.
[17] Hanson JA. Effects of curing and drying environments on splitting tensile strength of concrete. J Am Concrete Inst 1968;65(7):535–43.
[18] Fouré B. Note sur la chute de résistance à la traction du béton léger consécutive à l'arrêt de la cure umide. Ann Inst Tech Bâtiment Travaux Publics 1985;432:3–14. [in French].
[19] De Larrard F, Bostvirronois JL. On the long term losses of silica fume high strength concretes. Mag Concrete Res 1991;43(155):124–9.

[20] Baroghel-Bouny V, Mainguy M, Lassabatere T, Coussy O. Characterization and identification of equilibrium and transfer moisture properties for ordinary and high-performance cementitious materials. Cement Concrete Res 1999;29:1225–38.
[21] Mainguy M, Coussy O, Baroghel-Bouny V. Role of air pressure in drying of weakly permeable materials. J Eng Mech 2001;127(6):582–92.
[22] Meschke G, Grasberger S. Numerical modelling of coupled hygromechanical degradation of cementitious materials. J Eng Mech 2003;4:383–92.
[23] Bažant ZP, Chern JC. Concrete creep at variable humidity: constitutive law and mechanism. Mater Struct 1985;18(103):1–20.
[24] Mazars J. Application de la mécanique de l'endommagement au comportement non linéaire et à la rupture de béton de structure. PhD thesis, Paris, Paris VI University; 1984 [in French].
[25] Benboudjema F, Meftah F, Torrenti J-M. Interaction between drying, shrinkage, creep and cracking phenomena in concrete. Eng Struct 2005;27:239–50.
[26] Alvaredo AM, Wittmann FH. Shrinkage as influenced by strain softening and crack formation. In: Bažant ZP, Carol I, editors. Proceedings creep and shrinkage of concrete. London: E & FN Spon; 1993.
[27] Bažant ZP, Xi Y. Drying creep of concrete: constitutive model and new experiments separating its mechanisms. Mater Struct 1994;27:3–14.
[28] Hubert F-X, Burlion N, Shao J-F. Drying of concrete modelling of a hydric damage. Mater Struct 2003;36:12–21.
[29] Thiery M, Baroghel-Bouny V, Bourneton N, Villain G, Stefani C. Modélisation du séchage des bétons: analyse des différents modes de transfert hydrique. Rev Eur Génie Civil 2007;11(5):541–77. [in French].
[30] van Genuchten MTh. A closed-form equation for predicting the hydraulic conductivity of unsaturated soils. Soil Sci Soc Am 1980;44:892–8.
[31] Bažant ZP, Najjar LJ. Non linear water diffusion in non saturated concrete. Mater Struct 1972;5(25):3–20.
[32] Xi Y, Bažant ZP, Molina L, Jennings HM. Moisture diffusion in cementitious materials: moisture capacity and diffusivity. Adv Cement Based Mater 1994;1:258–66.
[33] Soroka I. Portland cement paste and concrete. Londres: Macmillan; 1979.
[34] Benboudjema F, Meftah F, Torrenti J-M. A viscoelastic approach for the assessment of the drying shrinkage behaviour of concrete. Mater Struct 2007;40(2):163–253.
[35] Gawin D, Pesavento F, Schrefler BA. Modelling creep and shrinkage of concrete by means of effective stresses. Mater Struct 2007;40:579–91.
[36] Carlson RW. Drying shrinkage of large concrete members. J Am Concrete Inst 1937;33:327–36.
[37] Torrenti J-M, Granger L, Diruy M, Genin P. Modeling concrete shrinkage under variable ambient conditions. ACI Mater J 1997;96(1):35–9.
[38] Bažant ZPWu ST. Rate-type creep law of ageing concrete based on Maxwell chain. Mater Struct 1974;7:45–60.
[39] Pickett G. The effect of change in moisture content on the creep of concrete under a sustained load. J Am Concrete Inst 1942;38:333–55.
[40] Acker P, Ulm -J. Creep and shrinkage of concrete: physical origins and practical measurements. Nucl Eng Des 2001;203:143–58.
[41] Reviron N, Benboudjema F, Torrenti J-M, Nahas G, Millard A. Coupling between creep and cracking in tension. In: Proceedings Framcos, vol. 6; 2007.
[42] Pijaudier-Cabot G, Bažant ZP. Nonlocal damage theory. J Eng Mech 1987;113:1512–33.
[43] Cervera M, Chiumenti M. Mesh objective tensile cracking via a local continuum damage model and a crack tracking technique. Comput Methods Appl Mech Eng 2006;196:304–20.
[44] Rots, JG. Computational modeling of concrete fracture. PhD thesis, Netherlands, Delft University of Technology; 1988.
[45] Feenstra PH, de Borst R. A composite plasticity model for concrete. Int J Solids Struct 1996;33(5):707–30.
[46] Granger L. Comportement différé du béton dans les enceintes de centrales nucléaires: analyse et modélisation. PhD thesis, Marne-La-Vallée, Ecole Nationale des Ponts et Chaussées; 1996 [in French].
[47] Commissariat à l'Energie Atomique CEA – DEN/DM2S/SEMT, Cast3m finite element code. <http://www-cast3m.cea.fr/>.
[48] Bourgeois F, Burlion N, Shao JF. Elastoplasticity and anisotropic damage due to drying shrinkage in concrete. In: Ulm F-J, Bažant ZP, Witmann FH, editors. Proceedings creep, shrinkage and durability mechanics of concrete and other quasi-brittle materials. Cambridge: Elsevier; 2001. p. 171–7.
[49] Rozière E, Granger S, Turcry Ph, Loukili A. Influence of paste volume on shrinkage cracking and fracture properties of self-compacting concrete. Cement Concrete Compos 2007;29(8):626–36.